Bulletin of Glaciological Research 17 (2000) 23－30

New passive microwave remote sensing technique for sea ice in the Sea of Okhotsk using 85-GHz channel of DMSP SSM/I

Kazutaka TATEYAMA[1], Hiroyuki ENOMOTO[1], Shuhei TAKAHASHI[1], Kazuyuki SHIRASAKI[1], Kinji HYAKUTAKE[1] and Fumihiko NISHIO[2]

1 Department of Civil Engineering, Kitami Institute of Technology, Kitami 090-8507 Japan

2 Hokkaido University of Education, 1-15-55 Shiroyama, Kushiro 085-8580 Japan

(Received March 4, 1999 ; Revised manuscript received June 14, 1999)

Abstract

A new sea ice classifying algorithm has been developed, based on aircraft measurements of the ice in Lake Saroma and in the Sea of Okhotsk by using a NASDA-developed Airborne Microwave Radiometer (AMR). This algorithm uses a parameter related to the 89-GHz channel of the AMR, which has the finer resolution, than the other channels. This high spatial resolution algorithm was applied to the Special Sensor Microwave/Imager (SSM/I) data, which has an 85-GHz channel for high spatial resolution (12.5×12.5 km^2), and was calibrated by comparing with NOAA AVHRR and ADEOS AVNIR visible and near infrared data. The spatial resolution of ice maps derived from this algorithm is 4 times greater per pixel than that of the NASA team algorithm, which uses only low spatial resolution (25×25 km^2) channels, 19, 22 and 37-GHz. Furthermore the false sea ice signals shown around the coast and marginal ice zone are decreased for all seasons by using this algorithm. This algorithm also attempts to classify sea ice types into fast ice, first-year ice, young ice and new ice by using the difference between the dielectric properties of 85-GHz and 37-GHz channels on different sea ice types with the thickness.

1. Introduction

1.1. Sea ice in the Sea of Okhotsk

The sea ice in the Sea of Okhotsk, which is one of the lowest latitude ice pack areas on the globe, consists entirely of first year ice. Observations by the SSM/I, that is part of an operational United States Defense Meteorological Satellite Program (DMSP) and have been continuing since 1987, have shown fluctuations of concentration and extent of ice (Nishio and Cho, 1996; Enomoto, 1996), and rapid decrease of ice extent, in the Sea of Okhotsk since 1989 (Tachibana *et al.*, 1996). However, in order to estimate the effect of global warming on sea ice, not only sea ice extent and concentration but also ice thickness should be analyzed because ice concentration might vary greatly due to the effect of wind, not only the thermal effect.

In the winter of 1996, a field experiment for sea ice observation, called the Sea Ice Observation Program in the Sea of Okhotsk (SIPSO), was carried out using an airborne passive microwave multi-channel radiometer over Lake Saroma and the eastern coast of Hokkaido. This report shows the results of development of a new algorithm based on the SIPSO experiment and applying the new algorithm to the DMSP SSM/I data over the whole Sea of Okhotsk.

1.2. Sea ice remote sensing

Although algorithms calculating ice concentration, such as the NASA team (Cavalieri *et al.*, 1991) algorithm and the Goddard Space Flight Center (GSFC) Bootstrap algorithm (Comiso *et al.*, 1992), are very useful tools in areas such as the Arctic and Antarctic, observation of sea ice in the Sea of Okhotsk involves some technical problems. The problems originate from false sea ice signals that come from atmospheric effects which turn up at low latitudes, and a coastal/land effect that contaminates the data due to the high ratio of land surrounding the sea (Cho *et al.*, 1996).

Cavalieri (1994) presented a technique for mapping the distribution of new, young and first-year ice in the Bering Sea from SSM/I. This technique used the polarization ratio (PR), which is sensitive to changes in ice thickness and ice surface characteristics, of 19-GHz and 37-GHz channels to classify ice types. PR varies with ice thickness from about 0.3 for open water, to about 0.15 for new ice, to 0.08 for young ice and to 0.03 for thick first-year ice. Although this technique has solved the problem, with thin ice signals regarded as multi-year ice in the seasonal ice areas, this technique still involves the problems of low resolution in the local area and confusion of concentration in the mixed ice types area.

The 85-GHz channels of SSM/I have a resolution of 12.5 km, twice the resolution of the other channels. However, the sea ice algorithms based on the DMSP SSM/I, the 19, 22 and 37-GHz, have been used for calculating ice concentration.

Sea ice classification experiments that have been done by airborne sensors and in laboratories have also used the higher frequency channels (Troy *et al.*, 1981; Eppler *et al.*, 1992; Wensnahan *et al.*, 1993). These experiments have shown that distinction of ice types by combining higher frequency channels with the other channels is possible .

2. Study area and method

2.1. Test sites

The Sea of Okhotsk used to freeze up to 80 % of total area until the 1980s, in the 1990s the sea ice area has occupied only below 60 % of the area (Nishio and Cho, 1996, Tachibana *et al.*, 1996). Lake Saroma, shown in Fig. 1, is a salt lagoon connecting to the Sea of Okhotsk by two mouths and has an area of 150.4km². This lagoon freezes up in winter; thus several sea ice experiments have been carried out in this lagoon.

2.2. Aircraft measurements

Observations, using a NASDA-developed Airborne Microwave Radiometer (AMR) mounted on a Beachcraft-200 (B-200), were carried out with ground measurements in Lake Saroma and the western coast of Hokkaido on the 17th of February, 1996. An airborne infrared radiometer was also used on the 15th and the 16th of February. The AMR has 6 channels (Table 1), each of which has vertical and horizontal polarization. This instrument was developed for the ground experiment related to the Advanced Microwave Scanning Radiometer (AMSR) on the ADEOS-II satellite, which will be launched in 2000.

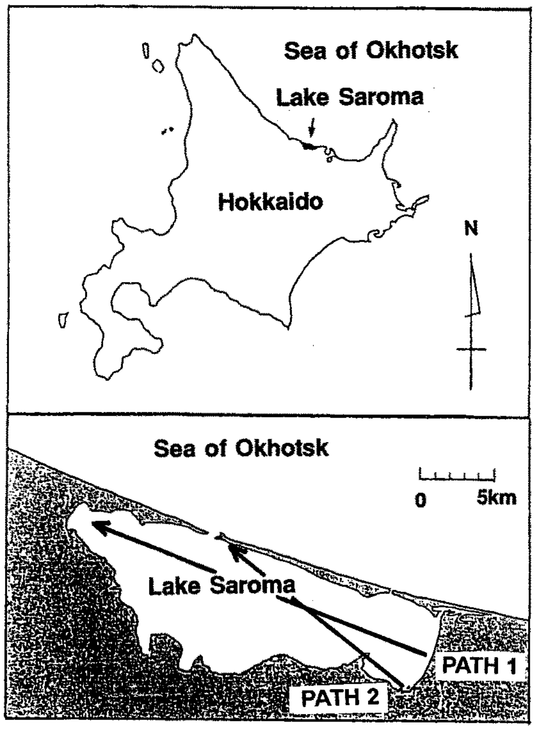

Fig. 1. Location of the Sea of Okhotsk and Lake Saroma.

Table 1. The channels of SSM/I, AMR and AMSR

Sensor	Channels (GHz)/Resolution (km)					
SSM/I			19.35	22.23	37.0	85.5
			25			12.5
AMSR	6.9	10.65	18.7	23.8	36.5	89.0
	50		25		15	5
AMR	6.9	10.65	18.7	23.8	36.5	89.0

In this study, the VTR images were taken from B-200 and used for the truth distribution data of the ice surface conditions, because the ice in the northwestern part of Lake Saroma was so thin that it was impossible to obtain the ground truth data over the whole lake. The drifting sea ice in the Sea of Okhotsk is also observed by used the VTR. From the VTR images the ice thickness distribution is assumed by watching surface color, size, snow cover and edge ridging.

3. Results

In Lake Saroma the ice thickness distribution was different between the northwestern and southeastern parts. VTR images show bare thin ice in the northwest, becoming thicker and covered by much snow in the southeast. In the southeast, the mean ice thickness and the mean snow cover were observed to be approximately 30 cm and 10 cm, respectively.

The general weather outlook was that air temperature increased to nearly 0 °C during the 11th and the 15th of February, and decreased rapidly to -18 °C on the 16th of February. So there should have been re-freezing on the ice surface in this period. On the 17th of February, the AMR observation was carried out. The air temperature remained below -10 °C throughout the day, hence the snow can be regarded as dry snow. Therefore the variation of brightness temperature derived from this experiment was related only to the variation of ice because the effect of snow cover was constant.

3.1. Sea ice signals

Figure 2 shows the distributions of brightness temperature, (a) from southeast to northwest (PATH-1) and (b) from land to ocean (PATH-2), received by each channel of the AMR and the infrared radiometer. The spike-like noises seen on each horizontal polar-

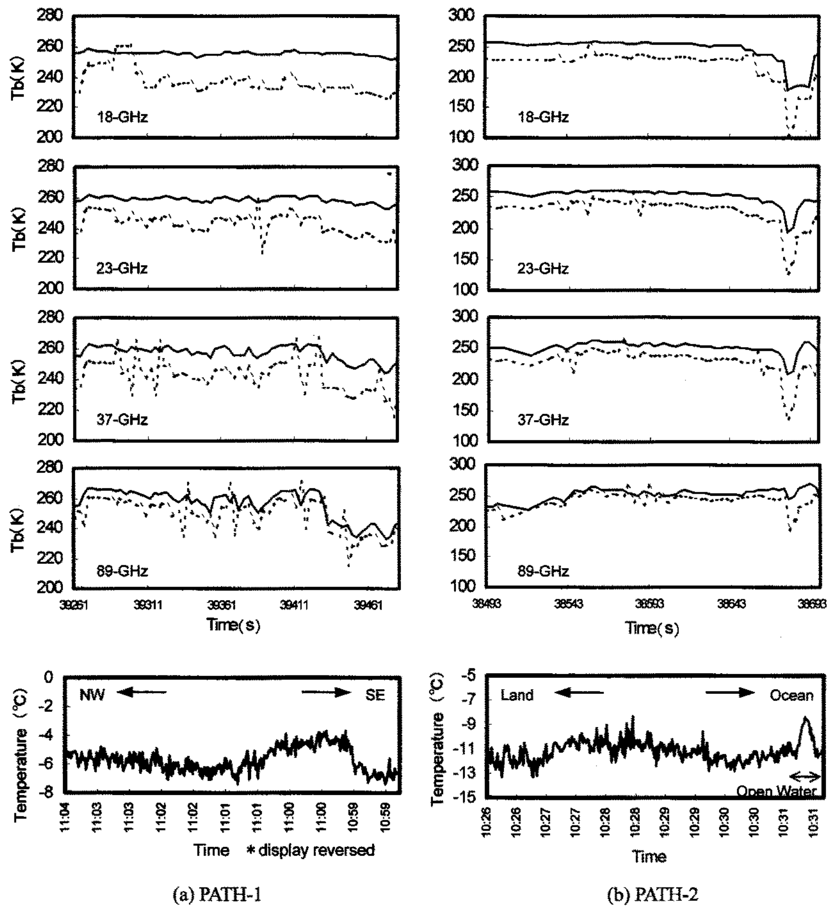

Fig. 2. Distributions of the brightness temperature on each channels of the AMR (V-pol: solid line, H-pol.: dashed line) on the 17th of February 1996 and infrared thermometer data.
(a) PATH-1 (SE-NW), ice surface temperature data were taken on the 15th of February,
(b) PATH-2 (from land to ocean), ice surface temperature data were taken on the 16th of February.

ized channel are assumed to be caused by interference from the electric waves.

It can be seen in the Fig. 2 that the horizontal polarization data shows large fluctuation and it increases with high frequency; and the difference between polarized channels decreases at higher frequency. The brightness temperature (T_B) of the vertically polarized 89-GHz channel varies greatly on ice and varies slightly on the open water.

Figure 2(a) indicates that the distribution of the 89-GHz channel signal varies with ice thickness and ice surface, from about 240 K on snow covered thick ice to about 270 K on bare thin ice. The signal of 89-GHz channels reflect the ice surface temperature because the variations are similar to those in the infrared radiometer data. In other words, the 89-GHz channel is more sensitive, even on continuous ice, than the other channels; this is assumed to reflect of ice thickness and surface differences.

Figure 2(b) shows significant decrease of T_B on open water, but on the vertically polarized 89-GHz the variation is so small that it is difficult to distinguish the open water signal.

3.2. Algorithm by using 89-GHz

This study uses the ratio between the vertically polarized 37-GHz (37V) and the vertically polarized 89-GHz (89V) of the AMR, designated $R_{37V/89V}$. The $R_{37V/89V}$ is used to obtain higher spatial resolution ability and to discriminate among ice types according to thickness.

The $R_{37V/89V}$ reflects the different radiometric properties between 37V and 89V and expresses the difference of ice thickness in the packed ice area, with concentration of 100 %. So when the $R_{37V/89V}$ is low in the packed ice area, the temperature of ice in the upper layer is assumed to be low, meaning that the ice is thick, and vice versa. On the other hand, although 89V is not able to differentiate open water as it indicate almost same brightness temperature as an ice, the $R_{37V/89V}$ can clearly discriminate the open water by using 37V, which is sensitive to the different dielectric constant between the ice and water. This difference between 37V and 89V on open water is larger than using that obtained 37V or another single channel, so that the $R_{37V/89V}$ is superior to find open water.

Figure 3 shows the results for the area covered by new ice, young ice and floe, off the eastern coast of Hokkaido. Fig. 3(a) uses the NASA team algorithm (Cavalieri, 1991), Fig. 3(b) uses $R_{37V/89V}$ instead of GR (spectral gradient ratio).

PR and GR are given by

$$PR = (T_{B19V} - T_{B19H})/(T_{B19V} + T_{B19H}) \qquad (1)$$

$$GR = (T_{B37V} - T_{B19V})/(T_{B37V} + T_{B19V}) \qquad (2)$$

PR is not only a good water/ice discriminator, but is also largely independent of the physical temperature of the radiating medium since it was the ratio of the observed radiance. GR is defined as a discriminator of ice type by using the differences of slopes between the brightness temperatures at 37-GHz and 19-GHz. As a result, PR gives ice concentration predominantly, GR gives the fraction of two ice types, which are first

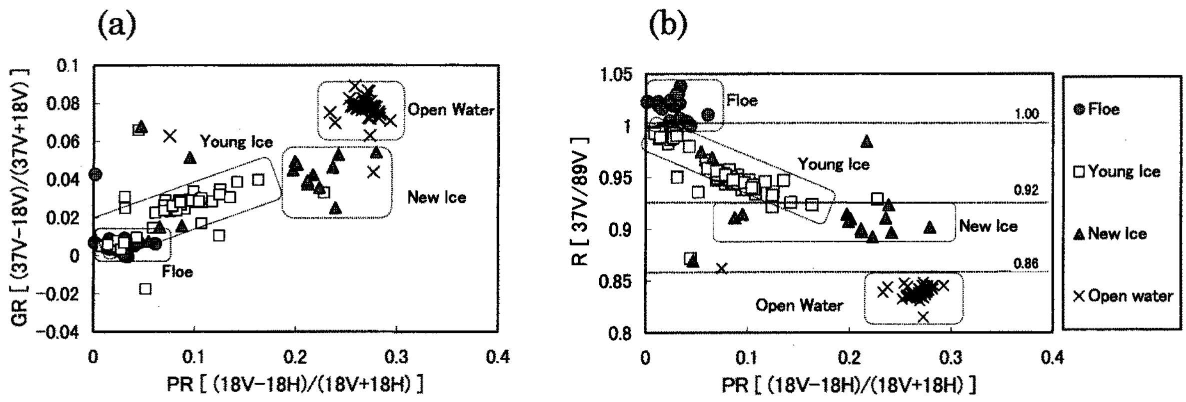

Fig. 3. Ice signal distribution, taken on the 17th of February 1996 in the Sea of Okhotsk.
(a) The NASA team Algorithm (PR-GR plane),
(b) PR-$R_{37V/89V}$ plane.

-year ice and multi-year ice in the Arctic. In the Antarctic, they consist of first-year ice and heavy snow covered ice (Cavalieri *et al.*, 1984; Markus and Cavalieri, 1998). The NASA team algorithm in the PR-GR plane is represented by a curvilinear triangle whose vertices are defined by 'tie points', which consist of the brightness temperature values for open water, first-year ice and multi-year ice in the Arctic (Cavalieri, 1991).

The results show that it is hard to distinguish young ice from floes by using the NASA team algorithm (Fig. 3(a)). On the other hand, when $R_{37V/89V}$ is used instead of GR, discrimination between ice floes and young ice can be done by using the $R_{37V/89V}=1.00$ line (Fig. 3(b)). Young ice and newly formed ice can be divided by $R_{37V/89V}=0.92$ and new ice and open water can be divided by $R_{37V/89V}=0.86$. The new ice, young ice and floes have thickness less than 10cm, 10～30cm and more than 30cm, respectively. This algorithm using the parameter $R_{37V/89V}$ is named the S/KIT (SIPSO/Kitami Institute of Technology) algorithm.

3.3. Application to SSM/I data

The S/KIT algorithm was applied to the SSM/I data in areas where the NASA team algorithm showed ice concentrations of more than 80% and those images are compared with the visible and near-infrared data of AVHRR on NOAA. By using the NASA-team algorithm, which has an ability to distinguish thin ice (Cavalieri, 1994), ice concentration (C) is calculated as a sum of concentration (C_A) of ice type A (first-year ice) and concentration (C_B) of ice type B (thin ice in terms of the Sea of Okhotsk), and is given by

$$C_A=(a_0+a_1PR+a_2GR+a_3PR\cdot GR)/a_0+a_1D, \quad (3)$$

$$C_B=(b_0+b_1PR+b_2GR+b_3PR\cdot GR)/D, \quad (4)$$

$$C=C_A+C_B \quad (5)$$

where

$$D= c_0+c_1PR+c_2GR+c_3PR\cdot GR. \quad (6)$$

The coefficients a_i, b_i, c_i ($i=0, 1, 2, 3$) of the NASA team Algorithm were modified for use in the Sea of Okhotsk as suggested by Enomoto (1996), as shown in Table 2. The weather filter for the Sea of Okhotsk, suggested by Cho *et al.* (1996), is used if GR> 0.05 and GR'>0.03, where GR' is given by

Table 2. The tie point values of the NASA team algorithm for the Sea of Okhotsk(Enomoto,1996)

Coefficients		
$a_0=$ 1255	$b_0=$ 687	$c_0=$-721
$a_1=$-10996	$b_1=$ 600	$c_1=$ 12936
$a_2=$ 18679	$b_2=$ 3417	$c_2=$-31260
$a_3=$ 30929	$b_3=$ 3504	$c_3=$-44918

$$GR'=(T_{B22V}-T_{B19V})/(T_{B22V}+T_{B19V}) \quad (7).$$

In such case, the concentration is substituted for 0 %. The vertically polarized 22-GHz (22V) channel is used to measure atmospheric effects because this channel is located in an absorption band of the atmosphere.

Figure 4 shows an example of a sea ice map which uses the S/KIT algorithm (Fig. 4(c)) and the concentration map uses the modified NASA team algorithm (the MNT algorithm) (Fig. 4(b)) and NOAA AVHRR image (Fig. 4(a)) on the 30th of March 1996. The MNT algorithm indicates the concentrated ice area (>80 % of ice concentration) with white. The lower concentration areas are indicated with a blue gradation, but their coverage is small. The S/KIT algorithm was applied only in the concentrated ice area calculated by using the MNT algorithm. The ice classifications are mapped in false colors (purple=floe; yellow=young ice; blue=low concentration area). If a distinct difference between the ice map and AVHRR images is found, then the threshold values of these areas are calibrated. Fast ice, which looks like a smooth surface and is a brighter white than floes, around the estuary of the Amur River, is colored red. New ice is distinguished from young ice by using the parameter $R_{19H/85V}$. This parameter uses the horizontal polarized 19-GHz (19H) to find the flat thin ice, which shows a relatively low brightness temperature on this channel because new ice such as nilas has a smooth surface. New ice is colored green. Shirasaki *et al.* (1998) observed a thin ice area along Sakhalin Island using the ADEOS AVNIR data. Young ice, floes and low concentration ice signals of the S/KIT algorithm are checked around the Terpeniya Peninsula on Sakhalin Island using their results as shown in Fig. 5.

The threshold values of the S/KIT algorithm, which are calibrated for the data taken from the SSM/I in the Sea of Okhotsk is summarized in Table 3. In the more than 80 % ice concentration area each grid point value is calculated from a combination of different resolution channels with 25×25 km^2 and 12.5×12.5 km^2. The high spatial resolution channel

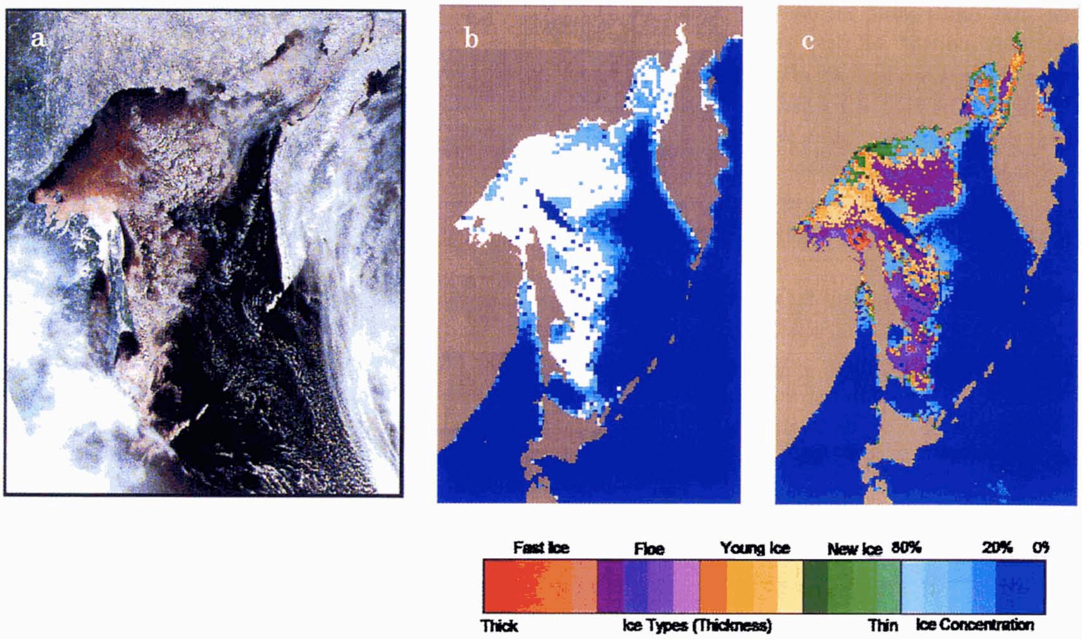

Fig. 4. Satellite Images on the 30th of March 1996.
(a) NOAA AVHRR composite image (Ch.1, Ch.2 and Ch.4),
(b) Sea ice concentration map by the NASA team algorithm,
(c) Sea ice concentration and classified map by the S/KIT algorithm.

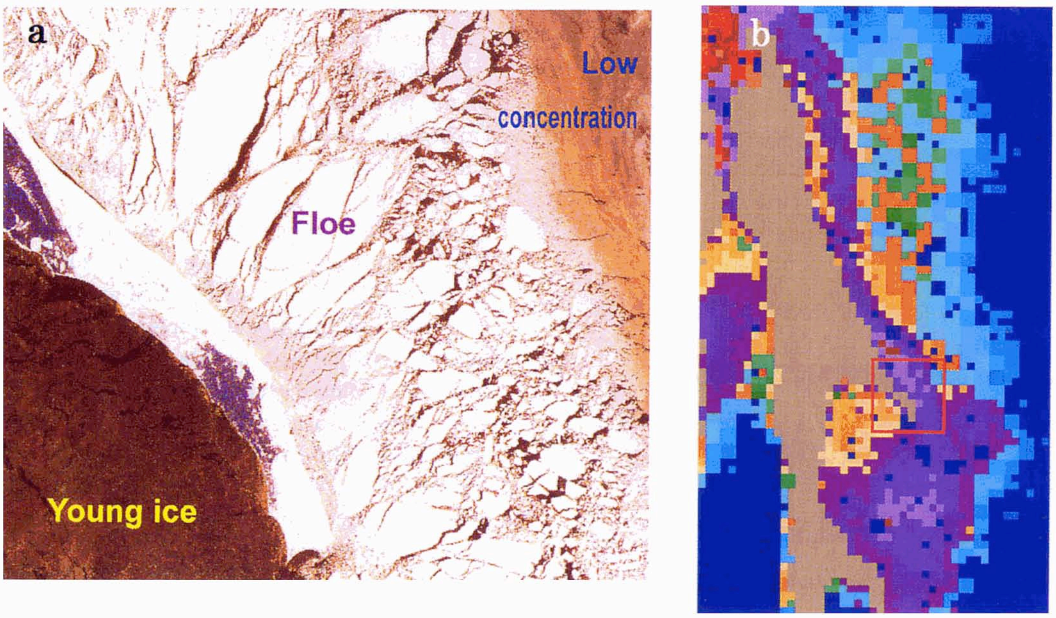

Fig. 5. Satellite images of the Terpeniya Peninsula in Sakhalin Island on the 7th of February 1997.
(a) ADEOS AVNIR, (b) Sea ice concentration and classified map by the S/KIT algorithm. The red square corresponds to Fig. 5(a).

Table 3. Threshold values of 85 and 37 GHz Ratio for four ice types, lower concentration area than 80% and open water.

Categories	Threshold Values
Fast Ice	$1.12 \leqq R_{37V/85V}$
Floe	$1.00 \leqq R_{37V/85V} < 1.12$
Young Ice	$0.97 \leqq R_{37V/85V} < 1.00$
New Ice	$0.92 \leqq R_{37V/85V} < 1.00$ and
	$0.20 \leqq R_{19H/85V} < 0.30$
Low Concentration	$0.92 \leqq R_{37V/85V} < 0.97$
Open Water	$R_{37V/85V} < 0.92$

varies greatly with the ice type in the packed ice area, hence grid point values change predominately on this channel and then have 12.5×12.5 km^2 resolvability.

3.4. Weather and land effect

It is necessary to remove the contamination in the ice signals originating from the atmosphere and the land in the Sea of Okhotsk. The contamination in the microwave sea ice signal is due to water vapor, clouds, rainfall and snowfall. The land effect causes a false ice signal due to the side-lobe of an antenna pattern when a field of view includes land. The land effect is serious for observing the coastal sea ice distribution. Although it is possible to remove the contamination from the atmosphere by using weather filters, it is impossible to separate the land contamination from the ice signal by merely an algorithm, due to this problem with antenna property and spatial resolution. However, it is possible to decrease the area affected by land noise by increasing the resolution. This study uses the weather filter suggested by Comiso (1994) but with a slightly lower value in the following threshold in Eq. (8). The concentration is set to be 0 % when

$$T_{B22V} - T_{B19V} > 12. \tag{8}$$

Significant improvement was obtained by reducing the land contamination. Fig. 6 compares the seasonal ice extent estimated by the MNT algorithm and the S/KIT algorithm for the Sea of Okhotsk during January and December 1996. Since there is no sea ice between June and the beginning of November, thus ice signals in this period are false. The false ice signals of the MNT algorithm in summer reach 10 % of the mean ice extent of winter; on the other hand, the S/KIT algorithm shows less than 3 %. Especially in summer in the Sea of Okhotsk, the S/KIT algorithm has less false ice, with the mean value 60 % lower and with the maximum value 80 % lower false signals than

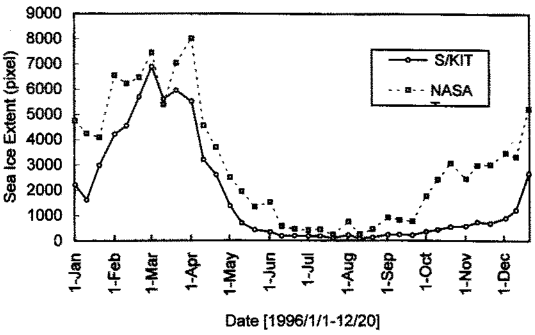

Fig. 6. Sea ice extent in the Sea of Okhotsk on the 1st of January and 30th of December 1996. The solid line shows the S/KIT algorithm and the dashed line shows the modified the NASA team algorithm. (unit: number of pixels. 1pixel: 12.5×12.5 km^2)

the MNT algorithm. Even in December and May, there are false signals due to the land contamination. The S/KIT algorithm reduces those false signals by applying the higher spatial resolution channel, while confirming the ice signal in the pixels of the lower spatial resolution channel (*i.e.* 37-GHz) along the coast and ice edge. Although there seems to be a seasonal variation in the land effect, its reason has not been confirmed. Consequently the large land effect in the early winter was reduced by applying the algorithm of this study.

4. Concluding remarks

This study discussed the possibility of the improved sea ice algorithm based on the field experiments in Hokkaido, and comparisons with NOAA AVHRR and ADEOS AVNIR images. The higher frequency channels of 85 or 89-GHz are useful for detecting ice type and also improving the higher spatial resolution and fewer false ice signals than the MNT algorithm. The AMSR board on ADEOS-II, which will be launched by NASDA in 2000, is expected to offer a higher-resolution view of the ice, since the 89-GHz channels of AMSR have 5 km spatial resolution.

The S/KIT algorithm still has low spatial resolution and false ice signals in the lower ice concentration area, because this area depends on only the NASA team algorithm in calculating the ice concentration. Therefore it is necessary to develop an algorithm calculating ice concentration using the 89 or 85-GHz channel. Analysis of the effect of snow cover on the ice, which contains more salinity than sea ice (Massom *et al.*, 1998), is also needed. Especially, the behavior of brightness temperature in melting season should be analyzed in detail, since water content and grain size of the snow layer over sea ice will increase and greatly affect microwave radiation in this season.

Acknowledgment

We would like to thank Prof. Peter M. Haugen and Prof. Yngvar T. Gjessing for their useful comments. We used AMR data and ADEOS AVNIR data provided by the National Space Development Agency of Japan (NASDA). SSM/I data were obtained from the National Snow and Ice Data Center (NSIDC) at Boulder, Colorado.

References

Cavalieri, D. J., P. Gloersen, and W. J. Campbell (1984): Determination of sea ice parameters with the NIMBUS 7 SMMR, J. Geophys. Res., **89**(D4), 5355-5369.

Cavalieri, D. J., J. P. Crawford, M. R. Drinkwater, D. T. Eppler, L. D. Farmer, R. R. Jentz, and C. C. Wackerman (1991): Aircraft active and passive microwave validation of sea ice concentration from the Defense Meteorological Satellite Program Special Sensor Microwave Imager, J. Geophys. Res., **96**(C12), 21,989-22,008.

Cavalieri, D. J. (1994): A microwave technique for mapping thin ice, J. Geophys. Res., **99**(C6), 12,561-12,572.

Cho, K., N. Sasaki, H. Shimoda, T. Sakata, and F. Nishio (1996): Evaluation and improvement of SSM/I sea ice concentration algorithms for Sea of Okhotsk, Jour. Remote Sensing Society of Japan, **16**(2), 47-58.

Comiso, J. C., T. C. Grenfell, M. Lange, A. Lohanick, R. Moore, and P. Wadhams (1992): Microwave remote sensing of the Southern Ocean ice cover, Passive microwave signatures of sea ice, In Carsey, F. D. (ed.), Microwave remote sensing of sea ice, Geophys. Monogr, **68**, 243-259.

Comiso, J. C. (1994): Ice concentration derived using the bootstrap algorithm, NSIDC Letter attached to revised CD-ROM.

Enomoto, H. (1996): Observation of thin ice area in the Okhotsk Sea and impacts for climatological study, Jour. Remote Sensing Society of Japan, **16**(2), 14-25.

Eppler D. T., L. D. Farmer, A. W. Lohanick, M. R. Anderson, D. J. Cavalieri, J. Comiso, P. Gloersen, C. Garrity, T. C. Grenfell, M. Hallikainen, J. A. Maslanik, C. Matzler, R. A. Melloh, I. Rubinstein, and C. T. Swift (1992): Passive microwave signatures of sea ice, In Carsey, F. D. (ed.), Microwave remote sensing of sea ice, Geophys. Monogr, **68**, 47-71.

Markus T. and D. J. Cavalieri (1998): Snow depth distribution over sea ice in the Southern Ocean from satellite passive microwave data, In Jeffries, M. O. (ed.), Antarctic sea ice: Physical processes, interactions and variability, Antarct. Res. Ser., **74**, 19-39

Massom, R. A., V. I. Lytle, A. P. Worby, and I. Allison (1998): Winter snow cover variability on East Antarctic sea ice, J. Geophys. Res., **103**(C11), 24,837-24,855.

Nishio, F. and K. Cho (1996): Sea ice extents in the Okhotsk Sea -improvement for sea ice concentration and climatic interpretation, Jour. Remote Sensing Society of Japan, **16**(2), 26-31, 1996.

Shirasaki, K., H. Enomoto, K. Tateyama, H. Warashina, and A. Watanabe (1998):Observation of sea ice conditions using visible and near-infrared channels in MOS-1/MESSR and ADEOS/AVNIR, Polar Meteorol. Glaciol., **12**, 86-96.

Tachibana, Y., M. Honda, and K. Takeuchi (1996): The abrupt decrease of the sea ice over the southern part of the Sea of Okhotsk in 1989 and its relation to the recent weakening of the Aleutian low, J. Meteorol. Soc. Japan, **74**(4), 579-584.

Troy, B. E., J. P. Hollinger, R. M. Lerner, and M. M. Wisler (1981): Measurement of the microwave properties of sea ice at 90 GHz and lower frequencies, J. Geophys. Res., **86**(C5), 4283-4289.

Wensnahan, M., G. A. Maykut, T. C. Grenfell, and D. P. Winebrenner (1993): Passive microwave remote sensing of thin sea ice using principal component analysis, J. Geophys. Res., **98**(C7), 12,453-12,468.